JOURNAL OF COMPUTATIONAL PHYSICS 114, 45–58 (1994)

On Essentially Non-oscillatory Schemes on Unstructured Meshes: Analysis and Implementation

R. ABGRALL

INRIA, BP 93, 06902 Sophia Antipolis Cedex, France

Received January 11, 1993; revised September 24, 1993

During the past few years, the class of essentially non-oscillatory schemes for the numerical simulation of hyperbolic equations and systems has been constructed. Since then, a few extensions have been made to multidimensional simulations of compressible flows, mainly in the context of very regular structured meshes. In this paper, we first recall and improve the results of an earlier paper about non-oscillatory reconstruction on unstructured meshes. We put much emphasis on the effective calculation of the reconstruction. Then, we describe a class of numerical schemes on unstructured meshes. We give some applications for its third order version. They demonstrate that a higher order of accuracy is indeed obtained, even on very irregular meshes.

1. INTRODUCTION

During the past few years, a growing interest has emerged for building high order accurate and robust schemes for compressible flows simulations. One of the difficulties is the appearance of possibly strong discontinuities that may interact together, even for smooth initial data. To eliminate this difficulty, a possible solution is to use a totally variation diminishing scheme. Such a scheme has the property, at least for 1D scalar equation, not to create new extrema and, hence, to provide a nice treatment of discontinuities. They have been since successfully and widely used with any type of meshes (see, for example, [1] for a review and, among many others, [2] for simulations on finite elements type meshes). Nevertheless, one of their main weaknesses is that the order of accuracy falls to first order in regions of discontinuity and at extrema, leading to excessive numerical dissipation.

Various methods have been proposed to overcome this difficulty (adaptation of the mesh, for example, see [3–5]) but one promising way may also be the class of the essentially non-oscillatory schemes (ENO for short) introduced by Harten, Osher, and others [6–10].

The basic idea of ENO scheme is to use a Lagrange type interpolation with an adapted stencil: when a discontinuity is detected, the procedure looks for the region around this discontinuity where the function is the smoothest. This reconstruction technique may be applied either to the node values [9] or to a particular function constructed from the averages in control volumes [6–8]. In this latter case, the approximation is done in such a way that it is conservative. This enables us to approximate any piecewise smooth function at any desired order of accuracy.

Up to now, very few attempts have been done to adapt these ideas to multidimensional flows, see, for example, [9, 11] for smoothly varying grids and much less on unstructured grids. For the latter topic, only preliminary works exist (see [12–14, 16]). In [14], together with a review of the existing ENO methods, an extension to general unstructured meshes is proposed. In particular, the problem of the reconstruction is considered with many details. The authors use the same polynomial approximation as us, but the selection of the stencil is completely different because they utilize a general unstructured mesh (with possibly several kinds of elements), thus the properties of its connectivity cannot be used as here. Because of that, they cannot give any bounds on the number of potential stencil for a given cell, contrary to the present paper. This is important because it is directly related to the cost of the algorithm. Experimental results obtained with this class of schemes are provided in [15]. In [16], several algorithms are presented and tested on simple problems (linear advection, Burger's like equations), but their reconstruction algorithms appear to be very complicated and costly. There is no study of the numerical stability of the reconstruction. Our experiences have shown that this point is fundamental. In [12], we have studied two reconstruction methods based on two different polynomial approximations; we have also estimated the behavior of their leading coefficients. This enables us to design an algorithm that has been tested for third- and fourth-order approximation. We also have discussed the choice of candidate stencils: a small number is sufficient. In [13], this reconstruction method has been implemented for compressible flow problems and tested on

0021-9991/94 $6.00

a 2D shock tube problem on a triangular mesh. In this finite volume scheme, the control volumes are the triangles of the mesh. If one wants this set as isotropic as possible, the minimum number of possible stencils is much larger than in the version presented in [12]; its construction is also less natural. This makes the scheme of [13] very costly.

This paper is organized as follows: in Section 2, we recall and improve the results obtained in [12]. Let us mention that these results are valid, whatever the type of the underlying mesh (structured or not). In particular, we pay much attention to the study of the numerical stability of the reconstruction algorithm. In Section 3, we present our numerical scheme. In Section 4, some numerical results are presented. Last, several general comments are done in the conclusion. Throughout this paper, the data are the mean values on given control volumes.

2. THE RECONSTRUCTION PROBLEM ON UNSTRUCTURED MESHES

Let us first recall basic facts about 1D reconstruction. They will enlighten why a new method has to be introduced in the context of unstructured meshes. We first recall how to interpolate data in an essentially non-oscillatory Lagrange type fashion and then how this is used to reconstruct 1D data.

The essentially non-oscillatory interpolation. It relies on two well-known properties of divided differences. Let $\{y_0 < y_1 < \cdots < y_k\}$ be a stencil and consider $[y_0, ..., y_k]\, v$, the $(k+1)$th divided difference of v, a piecewise smooth function real valued function.

1. If v is $p \geqslant n$ times continuously differentiable in the interval $[y_0, y_k]$, then

$$[y_0, ..., y_k]\, v = v^{(k)}(\xi_k)/k! \qquad \text{for all} \quad k \leqslant n$$
$$\text{and some} \quad \xi_k \in [y_0, y_k]$$

2. If $v^{(p)}$, $p < n$, admits a jump $[v^{(p)}]$ in $[y_0, y_k]$, then

$$[y_0, ..., y_k]\, v = O\left(\frac{[v^{(p)}]}{|y_k - y_0|^{k-p}}\right) \qquad \text{for all } k,$$
$$p+1 \leqslant k \leqslant n.$$

These relations express that the divided differences remain bounded whatever the mesh size for a smooth function but go to infinity more or less quickly for unsmooth ones. With the help of these two remarks, Harten *et al.* have derived the following ENO interpolation algorithm: let us give a grid $\{y_j\}$, $y_j < y_{j+1}$. For any j, first consider $\mathscr{S}^{(0)} = \{y_j\}$.

1. if $|[y_j, y_{j+1}]\, v| < |[y_{j-1}, y_j]\, v|$ then $\mathscr{S}^{(1)} = \{y_j, y_{j+1}\}$, else $\mathscr{S}^{(1)} = \{y_{j-1}, y_j\}$

2. assume that $\mathscr{S}^{(k)} = \{y_{j_0}, ..., y_{j_k}\}$, a stencil for $(k+1)$th-order reconstruction, is given (y_{j_0} and y_{j_k} are the extreme points of the stencil). If $|[y_{j_0-1}, y_{j_0}, ..., y_{j_k}]\, v| < |[y_{j_0}, ..., y_{j_k}, y_{j_k+1}]\, v|$ then $\mathscr{S}^{(k+1)} = \mathscr{S}^{(k)} \cup \{y_{j_0-1}\}$, else $\mathscr{S}^{(k+1)} = \mathscr{S}^{(k)} \cup \{y_{j_k+1}\}$.

Once the required number of points has been reached, one can compute Lagrange interpolation based on the last stencil of the algorithm: this is the ENO interpolation of v.

The 1D conservative reconstruction. We consider a mesh of $\mathbb{R}$, $\{x_i\}_{i \in \mathbb{Z}}$, that may be regular or not. Around each point, x_i, we define a control volume $[x_{i-1/2}, x_{i+1/2}]$, where as usual,

$$x_{i+1/2} = \frac{x_i + x_{i+1}}{2}.$$

Let us consider u, a piecewise smooth real valued function. We denote $\bar{u}_i$ the average of u in $[x_{i-1/2}, x_{i+1/2}]$:

$$\bar{u}_i = \frac{1}{x_{i+1/2} - x_{i-1/2}} \int_{x_{i-1/2}}^{x_{i+1/2}} u(t)\, dt. \tag{1}$$

There are two classical ways of reconstructing u from its averages:

1. *Reconstruction via primitive functions.* One consider W a primitive of u, say,

$$W(x) = \int_{x_{1/2}}^{x} u(t)\, dt.$$

The values of W at the points $x_{j+1/2}$ are easily recovered from the data:

$$W(x_{i+1/2}) = \sum_{j=0}^{i} (x_{j+1/2} - x_{j-1/2})\, \bar{u}_j.$$

One computes an essentially non-oscillatory reconstruction $R(W, n+1)$ of W, up to the order $n+1$, as explained above. Here, one sets $y_j = x_{j+1/2}$. The reconstruction of u, $R(u, n)$ is defined as

$$R(u, n) = \frac{dR(W, n+1)}{dx}.$$

Clearly, the average values of $R(u, n)$ over any $[x_{i-1/2}, x_{i+1/2}]$ is $\bar{u}_i$.

2. *Reconstruction via deconvolution.* Here, the mesh *must* be regular, $x_{i+1/2} - x_{i-1/2} = \Delta x$. One may see Eq. (1) as the convolution product v of u and the characteristic function of $[-\Delta x/2, \Delta x/2]$. One has $v(x_i) = \bar{u}_i$. Then v is reconstructed in an essentially non-oscillatory fashion as

explained above, where $y_j = x_j$. Finally, one applies a deconvolution operator to $R(v, n)$ as in [6], for example, to obtain $R(u, n)$.

Atkins and Casper [11] have used a tensor product of 1D reconstruction to derive their numerical scheme. This is possible because they assume a regular transformation between a Cartesian mesh of $[0, 1] \times [0, 1]$ and their computational grid. The same trick has been used in Shu *et al.* [9]. In the context of unstructured grid, these tricks cannot work for at least two reasons:

1. The reconstruction via deconvolution needs very regular meshes (each control volume can be obtained from any other by translation),

2. The reconstruction via primitive function methods needs to know point values of a primitive over any *rectangle* from the data. Hence, these rectangles must be exactly covered by control volumes. As it can be seen in Fig. 1, this is, in general, impossible.

These two remarks show that a straightforward extension of one-dimensional ideas is not sufficient for our purpose.

2.1. Preliminaries

In the sequel, the symbol $\mathbb{R}_n[X, Y]$ denotes the set of polynomials P in the variables X and Y of total degree less or equal to n:

$$P(X, Y) = \sum_{l=0}^{n} \sum_{i+j=l} a_{ij} X^i Y^j.$$

The set $\mathbb{R}_n[X, Y]$ is a vector space of dimension $N(n) = (n+1)(n+2)/2$, a basis of which is the set of monomials

$$\{(X - x_0)^i (Y - y_0)^j\}_{i+j \leqslant n},$$

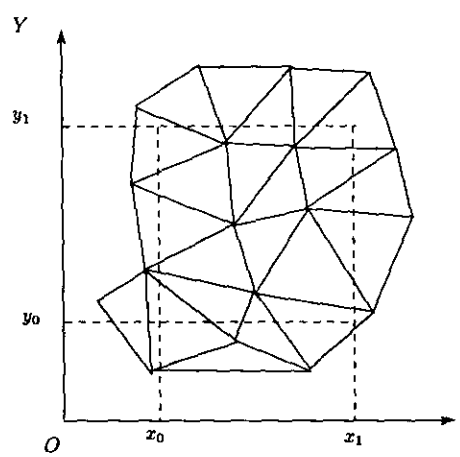

FIG. 1. Covering of the rectangle $[x_0, x_1] \times [y_0, y_1]$ by triangular control volumes.

where (x_0, y_0) is any point of $\mathbb{R}^2$. The total degree of P does not depend on the choice of (x_0, y_0). As we will show later, this kind of basis is not the best-suited for practical calculations.

Let $\mathcal{M}$ be a mesh of the finite element type. Associated with this mesh, we also consider a triangulation $\mathcal{T}$. We may consider several kind of control volumes, for example, the triangles of $\mathcal{T}$ themselves or the dual mesh (see Fig. 2). They are constructed as follows: for each point M_i, the control volume is obtained by connecting the midpoints of the segments adjacent to it and the barycenter of the triangles of which it is a vertex. Let us denote by $\{C_i\}$ the set of control volume. We only require the following properties:

- For any $i \neq j$, $C_i \cap C_j$ is of empty interior,
- C_i is connected and has a polygonal boundary,
- the vertices of the boundary of C_i depends continuously on the nodes of the mesh $\mathcal{M}$. This is true for the two examples above.
- The boundary of C_i is a locally regular curve. This is also true for the two examples above.

We consider the following problem (problem $\mathcal{P}$ or approximation in the mean for short):

Let u be a regular enough function (say in L^1). Given N and n two integer numbers, a set of control volumes $\mathcal{S} = \{C_{i_l}\}_{1 \leqslant l \leqslant N}$, find a element $P \in \mathbb{R}_n[X, Y]$ such that for $1 \leqslant l \leqslant N$,

$$\langle u \rangle_{C_{i_l}} \overset{\text{def}}{=} \frac{\int_{C_{i_l}} u \, dx}{\text{area}(C_{i_l})} = \langle P \rangle_{C_{i_l}}. \tag{2}$$

This solution admits a unique solution if and only if:

- $N = (n+1)(n+2)/2 = N(n)$

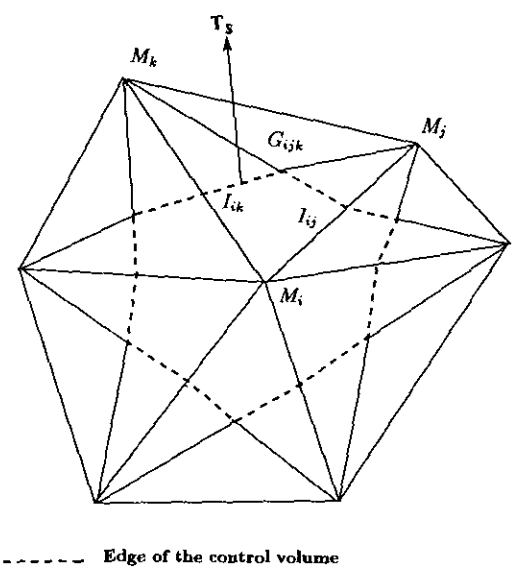

FIG. 2. Element of the dual mesh.

• the following Vandermonde type matrix is non-singular:

$$\mathscr{V} = [\langle X^i Y^j \rangle_{C_l}]_{\substack{i+j \leqslant n \\ 1 \leqslant l \leqslant N}} = \begin{bmatrix} 1 & \langle X \rangle_{C_1} & \langle Y \rangle_{C_1} & \cdots & \langle X^n \rangle_{C_1} & \langle X^{n-1} Y \rangle_{C_1} & \cdots & \langle Y^n \rangle_{C_1} \\ \vdots & \vdots & \vdots & \vdots & \vdots & \vdots & \vdots & \vdots \\ 1 & \langle X \rangle_{C_N} & \langle Y \rangle_{C_N} & \cdots & \langle X^n \rangle_{C_N} & \langle X^{n-1} Y \rangle_{C_N} & \cdots & \langle Y^n \rangle_{C_N} \end{bmatrix}. \tag{3}$$

If $\Delta_{\mathscr{S}} = \det \mathscr{V} \neq 0$, then we will often say that this stencil is admissible. In that case, there is a unique solution to problem $\mathscr{P}$ that will be denoted by P_u.

A similar problem was first considered by Barth *et al.* [17] for smooth functions, then by Harten *et al.* [14], Vankeirsblick *et al.* [16], and Abgrall [12].

In the first three references [17, 14, 16], the authors consider overdetermined systems for two related reasons: the problem $\mathscr{P}$ does not always have a unique solution; its condition number is very bad. They claim that the condition number of the overdetermined system is better than that of problem $\mathscr{P}$ which easily justifies the extra cost of CPU and memory. In [12], the same approach as here was adopted, where the minimum number of stencils is used. To support that choice, we must note, as is explained in Remark 1, that (3) is generally not singular. Second, the condition number of the linear system mainly depends on the basis used for the polynomial expansion, as it is shown in Section 2.4. The basis that appears naturally in Taylor expansion is the only one considered in [17, 14, 16]. The condition number of the linear system can be shown to be of the order of h^{-n}, where n the degree of the polynomials and h is a measure of the size of the mesh, as is shown in Section 2.4. A much better choice can be made; it leads to a linear system for which the condition number is independent of h. Thus, we have favored this approach which has the advantage of simplifying the coding of the global scheme.

Remarks. 1. We do not know if the admissibility condition admits a geometric interpretation (except for $n = 1$). We do not even know whether there is a systematic way of constructing admissible stencils, as is the case for the Lagrange interpolation [18]. Nevertheless, one may say that, in general, any stencil is admissible; one may consider the equation $\Delta_{\mathscr{S}} = 0$ as an algebraic surface in $\mathbb{R}^{2\times k}$ for some integer k.[1] This surface is then of empty interior, from a topological point of view, so that if $\mathscr{S}$ is not admissible, one only has to change slightly the elements of $\mathscr{S}$ to obtain an admissible stencil. Nevertheless, the condition number of the linear system may be very bad. We will discuss that point in Section 2.4.

[1] This is because we have assumed an algebraic dependency on the control volumes in terms of the points of $\mathscr{M}$.

2. This admissibility condition is independent on the basis chosen for expanding the polynomial P.

2.2. Some General Results about the Approximation in the Mean

In this section, we give two results on the behavior of the expansion of P_u, the solution of problem $\mathscr{P}$ for a function u, in the regions where u is smooth or not. They generalize well-known properties on the Lagrange interpolation of 1D real valued functions that have been used as a cornerstone by Harten and his coauthors to design an essentially non-oscillatory reconstruction. We have to emphasise the fact that the reconstruction in the mean is *not* directly related to the Lagrange one. Throughout this section, if $\mathscr{S}^{(n)}$ is an admissible stencil for degree n, the symbol $K(\mathscr{S}^{(n)})$ denotes the convex hull of the union of the elements of $\mathscr{S}^{(n)}$.

2.2.1. *Case of a Smooth Function*

In [12], we have shown the following result. Its proof follows easily from Ciarlet and Raviart's proof on Lagrange and Hermite interpolation:

THEOREM 2.1. *Let $\mathscr{S}$ be an admissible (for degree n) stencil of $\mathbb{R}^2$, let h and ρ be respectively the diameter of $K(\mathscr{S})$ and the supremum of the diameters of the circles contained in $K(\mathscr{S})$. Let u be a function that admits everywhere in $K(\mathscr{S})$ a $(n+1)$th derivative $D^{n+1}u$ with*

$$M_{n+1} = \sup\{\|D^{n+1}u(x)\|; x \in K(\mathscr{S})\} < +\infty.$$

If P_u is the solution of problem $\mathscr{P}$, then for any integer m, $0 \leqslant m \leqslant n$,

$$\sup\{\|D^m u(x) - D^m P_u(x)\|; x \in K(\mathscr{S})\} \leqslant C M_{n+1} \frac{h^{n+1}}{\rho^m}$$

for some constant $C = C(m, n, \mathscr{S})$. Moreover, if $\mathscr{S}'$ is obtained from $\mathscr{S}$ by an affine transformation (i.e., there exists $x_0 \in \mathbb{R}^2$ and A an invertible matrix such that

$$C'_k \in \mathscr{S}' \text{ iff there exists } C_k \in \mathscr{S} \text{ such that } C'_k = AC_k + x_0)$$

then

$$C(n, m, \mathscr{S}) = C(n, m, \mathscr{S}').$$

This result basically expresses that if the stencil $\mathscr{S}$ is not too flat, i.e., the ratio h/ρ is not too large, then P_u will be a good approximation of u. Let us turn now to the case of unsmooth functions.

2.3. Case of an Unsmooth Function

We only discuss the case of piecewise smooth functions. This is large enough for our purpose. To do the analysis, we

have to introduce the following property which prevents geometrical degeneration.

Property 2.2. Let us give $\varepsilon > 0$. The admissible stencil $\mathscr{S}^{(n)}$ belongs to $\mathscr{P}_\varepsilon^n$ if and only if the following property is true: Let u be any function the average of which on any element of $\mathscr{S}^{(n)}$ is either 0 or 1. Moreover, one assumes that there exists an element $C_{i_0} \in \mathscr{S}^{(n)}$ such that $\langle u \rangle_{C_{i_0}} = 1$ and an element $C_{i_1} \in \mathscr{S}^{(n)}$ such that $\langle u \rangle_{C_{i_1}} = 0$; hence P_u is non-constant. Then P_u is exactly of degree n and the sum of the absolute values of its coefficients of degree n is larger than ε.

Then we can prove [12] the following theorem that describes the asymptotic behavior of the leading coefficients of the approximation in the mean of a piecewise smooth function.

THEOREM 2.3. *Let ε be a positive real number and $\mathscr{S}^{(n)}$ an admissible stencil for degree n such that there exists an affine transformation $\mathscr{A}$ as in Theorem* 2.1 *for which $\mathscr{A}(\mathscr{S}^{(n)}) \in \mathscr{P}_\varepsilon^n$. Let (x_0, y_0) be any point of the set $K(\mathscr{S}^{(n)})$ and u a real valued function defined on a open subset Ω of $\mathbb{R}^2$ containing $K(\mathscr{S}^{(n)})$. We assume that u is C^{p-1}, $p < n$, in Ω and, except on a locally C^1 curve, admits a continuous and bounded pth derivative with a jump $[D^p u]$, $|[D^p u]| > M_p > 0$. Then, the highest degree coefficients of the Taylor expansion of P_u satisfies*

$$\sum_{i+j=n} |a_{ij}| \geqslant C(n, p, \varepsilon) \frac{M_p}{h^{n-p}}, \tag{4}$$

where $C(n, p, \varepsilon)$ is a constant independent of $\mathscr{S}^{(n)}$ and invariant by affine transformation.

This result tells us that in the vicinity of a discontinuity curve that is smooth enough, then the leading coefficients of P_u will tend to infinity as the mesh size tends to zero, while in the area where u is smooth enough, these coefficients *always* remain bounded. These two results are exactly the ones that have been used to derive the 1D ENO reconstruction algorithms by Harten *et al.* Now we have to answer an important question, how do we compute safely these polynomials?

2.4. Study of the Linear Problem to Solve for the Reconstruction

In this section, we intend to study the numerical system to solve for P_u from the data. We will consider two kinds of expansion of P_u:

1. the "natural" expansion for any point $(x_0, y_0) \in \mathbb{R}^2$,

$$P_u = \sum_{i+j \leqslant n} a_{ij} (X - x_0)^i (Y - y_0)^j \tag{5}$$

2. an expansion using "barycentric" coordinate that we describe now: let $\mathscr{S}^{(n)} = \{C_1, C_2, C_3, ..., C_{N(n)}\}$ be an admissible stencil. Hence, at least one subset of three elements of $\mathscr{S}^{(n)}$ is an admissible stencil for $n = 1$. We may assume that the set $\{C_1, C_2, C_3\}$ is admissible. We consider the three polynomials Λ_i of degree 1, defined by

$$\langle \Lambda_i \rangle_{C_j} = \delta_i^j, \qquad 1 \leqslant i \leqslant 3, \qquad 1 \leqslant j \leqslant 3. \tag{6}$$

The symbol δ_i^j is the Kronecker symbol. Clearly, we have $\Lambda_1 + \Lambda_2 + \Lambda_3 = 1$. These polynomials are the barycentric coordinates of the triangle constructed on the gravity centers of C_1, C_2, and C_3. In order to obtain expansion (5), a strategy may be to look first for the expansion of the polynomial P_u in terms of power of Λ_2 and Λ_3,

$$P = \sum_{i+j \leqslant n} a_{ij} \Lambda_2^i \Lambda_3^j, \tag{7}$$

and then to obtain the Taylor expansion of P_u around the barycenter of C_1 from (7) (Theorems 2.1 and 2.3 give the behavior of the leading coefficients of P_u, whatever the point chosen in the convex hull of $\mathscr{S}$).

In order to obtain the expansions (5) or (7), one has to solve linear $N(n) \times N(n)$ systems,

$$\mathscr{B}(a_{00} \cdots a_{0n})^{\mathrm{T}} = (\langle u \rangle_{C_{i_1}} \cdots \langle u \rangle_{C_{i_{N(n)}}})^{\mathrm{T}}, \tag{8}$$

where the matrix $\mathscr{B}$ is obtained by taking the average of $(X - x_0)^i (Y - y_0)^j$ for (5) and $\Lambda_2^i \Lambda_3^j$ for (7). The lexicographic ordering is adopted, so that the coefficient a_{ij} refers to $(X - x_0)^i (Y_{y_0})^j$ or $\Lambda_2^i \Lambda_3^j$. Let us now study the properties of these linear systems.

2.4.1. *Case of Expansion* (5)

A very easy consequence of the inequality (4) is that:

PROPOSITION 2.4. *Let us assume that the conditions of Theorem* 2.3 *hold, and let h be the supremum of the diameters of the spheres containing $K(\mathscr{S}^{(n)})$. Then the condition number of system* (8) *is at least $O(h^{-n})$ for h small enough.*

Proof. For the sake of simplicity, we consider the following norm on $\mathbb{R}_n[X, Y]$; for $P = \sum_{i+j \leqslant n} a_{ij} (X - x_0)^i (Y - y_0)^j$, $\|P\| = \sum_{i+j \leqslant n} |a_{ij}|$. On $\mathbb{R}^{N(n)}$, we consider the L^1 norm. Let U be a set of data for the right-hand side of (8) and consider the perturbation δU,

$$\delta U = (0 \cdots \varepsilon \cdots)^{\mathrm{T}},$$

where ε is in the lth position, $l \geqslant N(n-1) + 1$. All the other entries of U are zero. If one considers the function u defined on $\bigcup \mathscr{C}_i$ by

$$x \in C_i, \qquad u(x) = \delta U_i,$$

one can apply Theorem 2.3. Hence, the perturbation δP has a norm satisfying

$$\|\delta P\| \geqslant \sum_{i+j=n} |\delta a_{ij}| \geqslant C \frac{\varepsilon}{h^n}$$

since $\|\delta U\| = \varepsilon$. This complete the proof. ∎

This fact is well known for 1D Lagrange interpolation and has motivated the search of more efficient algorithms, such as the Newton algorithm. There exist algorithms that generalize it [19, 20]. They involve numerous solutions of linear systems, so that we have preferred a more classical approach (see Section 2.5), for which the coefficients of the linear systems are obtained from the "barycentric" coordinate expansion (7) as is explained now.

2.4.2. *Case of Expansion* (7)

In the case of expansion (7), we have the following result:

PROPOSITION 2.5. *If Property* 2.2 *holds for some* $\varepsilon > 0$, *then the condition number of the system* (8) *for the expansion* (7) *is bounded above and below by constants independent of* h, *the supremum of the diameters of the circles containing* $K(\mathscr{S}^{(n)})$.

Proof. The proof is also based on that of Theorem 2.3. As in Proposition 2.4, the only thing that we have to do is to study the effect on the a_{ij}'s of a perturbation δU. We denote by P the polynomial which averages are defined by δU. The proof can be achieved in two stages:

1. Let B be any invertible matrix. Consider the stencil

$$\widehat{\mathscr{S}^{(n)}} = \{B[C_{ij}] + x_0\}_{1 \leqslant j \leqslant N(n)}$$

for any x_0. It is clear, from the definition of the Λ_i's that $\hat{\Lambda}_i(\hat{x}) = \Lambda_i(x)$ if $\hat{x} = Bx + x_0$. Hence, the sum $S(P)$ of the absolute values of the coefficients of P in the basis $\Lambda_2^i(x)\,\Lambda_3^j(x)$ is the same as that of the development of P in the basis $\hat{\Lambda}_2^i(\hat{x})\,\hat{\Lambda}_3^j(\hat{x})$. This is an homogeneity property.

2. Since the set of stencils defined by Property 2.2 is compact, $S(P)$ is bounded below and above, independently of B, hence, independently of h:

$$C_1 \geqslant F \geqslant C_2(\varepsilon, n) > 0.$$

The constant $C_2(\varepsilon, n)$ is larger than zero because $\delta U \neq 0$.

This achieves the proof. ∎

2.5. The Explicit Calculation of the Reconstruction

From the previous results, the evaluation of the coefficients a_{ij} in (5) is done through those of (7) and hierarchically. For the sake of simplicity, we assume that for any $p \leqslant n$, the set $\mathscr{S}^{(p)}$ of the $N(p)$ first elements of $\mathscr{S}^{(n)}$ is admissible for order p. This can be achieved with a suitable numbering of the elements of $\mathscr{S}^{(n)}$. The idea is, instead of looking directly for the coefficients of $P^{(n)}$, to obtain first those of all of the $P^{(k)}$'s, the reconstruction over $\mathscr{S}^{(k)}$, for $1 \leqslant k \leqslant n$ and then to construct those of $P^{(n)}$. In the ENO algorithm described in Section 2.6, this involves *no* extra cost and simplifies the evaluation of the a_{ij}'s. This has also the advantage of reducing the size of the linear systems and also of improving their condition number. Assume that $P^{(1)}, \ldots, P^{(p)}$ are known.

We first obtain the coefficients of $P^{(p+1)} - P^{(p)}$,

$$P^{(p+1)} - P^{(p)} = \sum_{i+j \leqslant p+1} a'_{ij} \Lambda_2^i \Lambda_3^j,$$

by solving the linear system

$$A_{p+1} \begin{pmatrix} \mathbf{a}_1 \\ \mathbf{a}_2 \end{pmatrix} = \begin{pmatrix} A_p & B_{p\,p+1} \\ C_{p\,p+1} & D_{p\,p+1} \end{pmatrix} \begin{pmatrix} \mathbf{a}_1 \\ \mathbf{a}_2 \end{pmatrix} = \begin{pmatrix} \mathbf{u}_1 \\ \mathbf{u}_2 \end{pmatrix} \tag{9}$$

In Eq. (9), $\mathbf{a}_1$ (respectively $\mathbf{a}_2$) stands for the coefficients $\{a_{ij}\}_{i+j \leqslant p}$ (resp. $\{a_{ij}\}_{i+j=p+1}$). The block matrices A_p, $B_{p\,p+1}$, $C_{p\,p+1}$, and $D_{p\,p+1}$ are defined according to this decomposition. In particular, we note from the hypothesis that A_p is invertible.

From the conservativity property, we obtain $\mathbf{u}_1 = 0$, so that the system (9) can be split:

$$\begin{aligned} \mathbf{a}_1 &= -A_p^{-1} B_{p\,p+1} \mathbf{a}_2 \\ [-C_{p\,p+1} A_p^{-1} B_{p\,p+1} + D_{p\,p+1}]\, \mathbf{a}_2 &= \mathbf{u}_2. \end{aligned} \tag{10}$$

Since $\mathscr{S}^{(p+1)}$ is admissible, $E_p = [-C_{p\,p+1} A_p^{-1} B_{p\,p+1} + D_{p\,p+1}]$ is also invertible, so that one can obtain $\mathbf{a}_2$, then $\mathbf{a}_1$, and, last, the coefficients of $P^{(p+1)}$.

Simple manipulations show that

$$A_{p+1}^{-1} = \begin{pmatrix} A_p^{-1} B_{p\,p+1} E_p^{-1} C_{p\,p+1} A_p^{-1} + A_p^{-1} & -A_p^{-1} B_{p\,p+1} E_p^{-1} \\ -E_p^{-1} C_{p\,p+1} A_p^{-1} & E_p^{-1} \end{pmatrix},$$

so that one can quite easily look for the next step. In our case, since the total degree of the reconstruction is less than or equal to 4, at most two stages of that method are needed.

Last, one must note that the condition number of that method is always better than the one of the original system; it depends only on the condition number of a part of it.

2.6. A Quasi Minimal Family of Potential Stencil for the ENO Reconstruction

In [12], we have found that only a small number of stencils was indeed necessary to achieve an essentially non-oscillatory reconstruction of a piecewise smooth function.

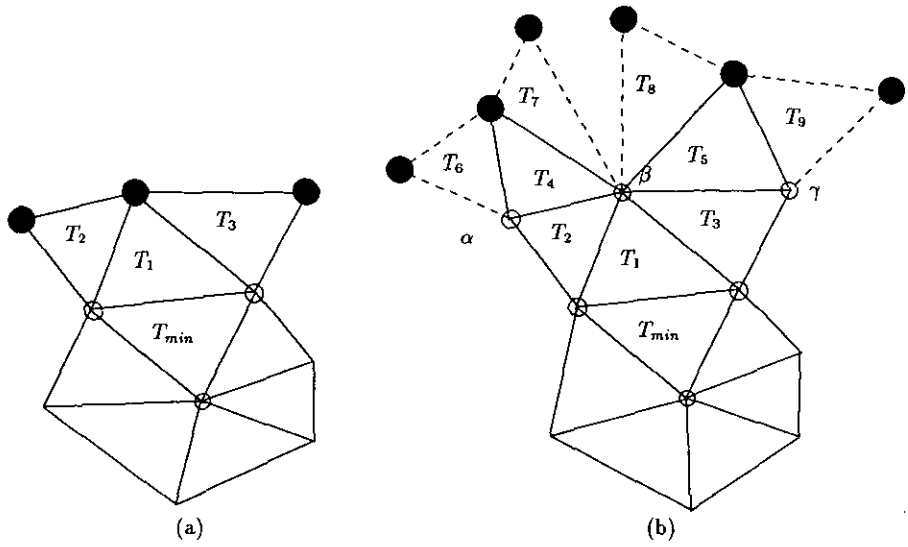

FIG. 3. Stencils for third- and fourth-order reconstruction.

This set has to be as isotropic as possible. Moreover, the ENO reconstruction was found to achieve the expected order of accuracy for smooth functions, even on very irregular meshes. In what follows, a_{ij} always stands for any of the coefficients of the reconstruction P in the natural basis, $\{(X-x_0)^i (Y-y_0)^j\}$. Let us describe our procedure up to fourth order:

1. Let us start from a given cell, C_0 assigned to a point of $\mathcal{M}$, say (x_0, y_0).

2. Consider all the triangles having (x_0, y_0) as a vertex and choose the one, say $T_{\min}$, that minimizes

$$\sum_{i+j=1} |a_{ij}|.$$

Here, $\mathcal{S}^{(1)}$ is the set of control volumes affected by the vertices of $T_{\min}$ (see Fig. 3a). For a regular unstructured mesh, there are of the order of six possible triangles.

3. Consider $T_{\min}$. For any of its three edges, consider the three triangles, T_1, T_2, T_3 as in Fig. 3a. There are three possible configurations. We choose the one that minimizes the sum

$$\sum_{i+j=2} |a_{ij}|.$$

4. Consider, as in Fig. 3b, the configuration for third order. It is obtained as follows: for a stencil $\mathcal{S}^{(2)}$ made of the control volumes associated to the vertices of $\{T_{\min}, T_1, T_2, T_3\}$, one may consider its "edges" made of the external sides of $\{T_2, T_3\}$, $\{T_2, T_{\min}\}$, $\{T_{\min}, T_3\}$. Consider one of them, say $\{T_2, T_3\}$, and the vertices α, β, and γ. Since the triangulation is conformal, there exists a triangle $T_4 \neq T_2$ on the other side of $[\alpha, \beta]$. Consider T_6 for $[\beta, \gamma]$. Then, for the same reasons, one can construct T_6, T_7, T_8, and T_9. The stencils for fourth-order reconstruction are the union of $\mathcal{S}^{(2)}$ and the control volumes associated to the additional vertices of either $\{T_4, T_5, T_6, T_7\}$ or $\{T_4, T_5, T_9, T_8\}$ or $\{T_4, T_5, T_7, T_8\}$. For a stencil $\mathcal{S}^{(2)}$, there are at most 12 stencils for fourth-order reconstruction.

The situation seems to become more and more complicated as the degree increases. Nevertheless, there is a very easy way to simplify it, so that at each level only three stencils for $(n+1)$th order have to be considered from a nth-order one, as we did from second order to third order. Let us give a mesh $\mathcal{M}$; we want to derive a $(n+1)$th-order reconstruction method. The idea is to work with the control volumes defined for a mesh $\mathcal{M}'$. For each triangle T of $\mathcal{M}$, we add the

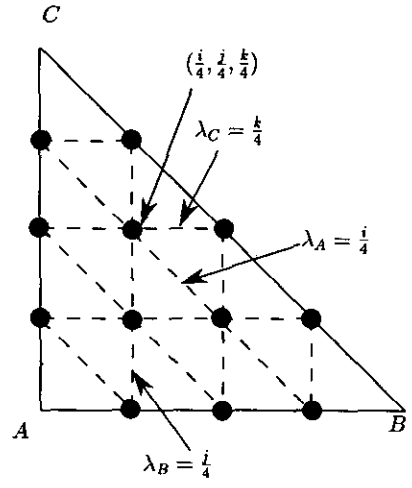

FIG. 4. Additional nodes (●) in (A, B, C) for $n=3$.

points and the triangles associated to the P_n Lagrange interpolation in T [21].

The additional points are constructed as follows. Any triangle of the coarse mesh can be mapped onto a rectangular triangle (A, B, C), as on Fig. 4. We denote by λ_A (resp. λ_B and λ_C) the barycentric coordinate toward A (resp. B and C) and consider the points A_{ij} which barycentric coordinates are $\lambda_A(A_{ij}) = i/(n+1)$, $\lambda_B(A_{ij}) = j/(n+1)$, and, of course, $\lambda_C(A_{ij}) = 1-(i+j)/(n+1)$. We request that i and j are positive integers such that $i+j>0$; thus the additional points are inside (A, B, C) and are different of A, B, and C. The new triangles are shaped as it is suggested on Fig. 4.

2.7. The ENO Reconstruction: Summary of the Method

Given a piecewise smooth function u and a cell C, the $(n+1)$th-order ENO reconstruction $R(u, n+1)$ of u in C is obtained after the following steps:

1. One has to define a family of potential stencils with the help of the algorithm presented in Subsection 2.6. This gives a set of stencils for each order p, $1 \leqslant p \leqslant n+1$, such that a stencil for order $p>2$ is constructed from a stencil for order $p-1$.

2. Starting from the family of stencils for second-order approximation, one looks for the triangle that minimizes the sum of the absolute values of the Taylor expansion of the linear reconstruction toward the gravity center of C.

3. Then, one looks for the family of stencils for third-order reconstruction that is constructed on the triangle that has been previously chosen. One chooses the stencils of that family that minimizes the absolute value of the highest degree coefficients of the Taylor expansion towards the same point.

4. One continues the procedure hierarchically up to the requested order of accuracy.

3. A CLASS OF HIGH ORDER NUMERICAL SCHEME FOR COMPRESSIBLE FLOW SIMULATIONS

3.1. The Euler Equations

Let us quickly recall elementary things about the Euler equation of a calorically perfect gas:

$$\frac{\partial W}{\partial t}+\frac{\partial F(W)}{\partial x}+\frac{\partial G(W)}{\partial y}=0. \tag{11}$$

As usual, in Eq. (11), W stands for the vector of conserved quantities and F (resp. G) is the flux in the x direction (resp. y direction):

$$W=\begin{pmatrix}\rho\\ \rho u\\ \rho v\\ E\end{pmatrix},\quad F(W)=\begin{pmatrix}\rho u\\ \rho u^2+p\\ \rho uv\\ u(E+p)\end{pmatrix},\quad G(W)=\begin{pmatrix}\rho v\\ \rho uv\\ \rho v^2+p\\ v(E+p)\end{pmatrix} \tag{12}$$

with initial and boundary conditions. In Eq. (12), ρ is the density, u and v are the components of the velocity, E is the total energy, and p the pressure, related to the conserved quantities by the equation of state:

$$p=(\gamma-1)(E-\tfrac{1}{2}\rho(u^2+v^2)). \tag{13}$$

The ratio of specific heats, γ, is kept constant.

It is well known that the system defined by Eqs. (11), (12), and (13) is hyperbolic: for any vector $\mathbf{n}=(n_x, n_y)$, the matrix

$$A_{\mathbf{n}}=n_x\frac{\partial F}{\partial W}+n_y\frac{\partial G}{\partial W} \tag{14}$$

is diagonalizable and has real eigenvalues and eigenvectors. Let us describe now the construction of a kth order scheme.

3.2. Finite Volume Formulation

We consider a mesh $\mathcal{M}$ and the control volumes as on Fig. 2. The semi-discrete finite volume formulation of (11) is

$$\frac{\partial}{\partial t}\bar{W}_i(t)=-\frac{1}{\text{area}(\mathcal{C}_i)}\int_{\partial\mathcal{C}_i}\mathcal{F}_{\mathbf{n}}[W(x,t)]\,dl=\mathcal{L}_i(t). \tag{15}$$

Here, $W(t)$ is the (spatial) mean value of $W(x, t)$ at time t over $\mathcal{C}_i$, $\mathbf{n}=(n_x, n_y)$ is the outward unit normal to $\partial\mathcal{C}_i$, and $\mathcal{F}_{\mathbf{n}}=n_xF+n_yG$. We first describe the spatial approximation of (15), then the temporal discretization of the resulting set of ordinary differential equations. Last, we detail the boundary conditions.

3.2.1. *Spatial Discretization*

For the sake of simplicity, we define the integer number p such that either $k=2p$ or $k=2p+1$. The first step is to

discretize $\mathscr{L}_i(t)$ up to kth order. First, we can rewrite area($\mathscr{C}_i$) $\mathscr{L}_i(t)$ as

$$\int_{\partial\mathscr{C}_i} F_{\mathbf{n}}[W(x,t)]\,dl = \sum_{\Gamma_s} \int_{\Gamma_s} F_{\mathbf{n}}[W(x,t)]\,dl, \tag{16}$$

where, as on Fig. 2, the Γ_s's are the edges of $\mathscr{C}_i$. On each Γ_s, $\mathbf{n}$ is constant. We consider, on any Γ_s, the p Gaussian points $\{G_l\}_{1\le l\le p}$ associated to the Gaussian formula of order $2p+1$. The integral $\int_{\Gamma_s} F_{\mathbf{n}}[W(x,t)]\,dl$ is approximated by

$$\sum_{l=1}^{p} \omega_l \mathscr{G}_{\mathbf{n},l}(t), \tag{17}$$

where $\mathscr{G}_{\mathbf{n},l}(t)$ is defined now. Set $\mathscr{C}_j$ to be the other control volume of which Γ_s is a part of the boundary. In $\mathscr{C}_i$ and $\mathscr{C}_j$, one computes the ENO reconstructions at time t of W, $R_i[W(\cdot,t),k]$ and $R_j[W(\cdot,t),k]$, up to order k. The ENO reconstruction of Section 2 is applied to the physical variables, then one deduces the conserved ones. From that, we set, in Eq. (17):

$$\mathscr{G}_{\mathbf{n},l}(t) = \mathscr{F}_{\mathbf{n}}^{\text{Riemann}}\{R_i[W(\cdot,t),k](G_l), R_j[W(\cdot,t),k](G_l)\}. \tag{18}$$

In Eq. (18), $\mathscr{F}_{\mathbf{n}}^{\text{Riemann}}$ may be any of the available Riemann solvers. In all the examples below, we have chosen Roe's Riemann solver with Harten–Hyman entropy correction.

3.2.2. *Temporal Discretization*

Equations (15), (16), (17), and (18) define a finite set of ordinary differential equations that we symbolize by

$$\frac{\partial}{\partial t}\bar{W}_i(t) = \tilde{\mathscr{L}}_i(t). \tag{19}$$

In (19), $\tilde{\mathscr{L}}_i(t)$ is the discrete version of $\mathscr{L}_i(t)$. This equation is discretized by the kth-order version of the Runge–Kutta scheme of Shu [9]:

$$W_i^{(l)} = \sum_{m=0}^{l-1} [\alpha_{lm} W_i^{(m)} + \beta_{lm} \tilde{\mathscr{L}}_i^{(m)}], \quad l = 1, 2, \ldots, p, \quad \tilde{\mathscr{L}}_i^{(m)} = \tilde{\mathscr{L}}_i(W_i^{(m)}) \tag{20}$$
$$W_i^{(0)} = W_i^n, \qquad W_i^{(p)} = W_i^{n+1}.$$

The order of accuracy, as well as its TVD properties, is achieved by adequate sets of coefficients α_{lm}, β_{lm}, and p (see [9] for details).

3.2.3. *Boundary Conditions*

Let Γ be the boundary of the computational domain and let $\mathbf{n}$ be the outward normal unit on Γ. We assume that Γ is divided in two parts, $\Gamma = \Gamma_0 \cap \Gamma_\infty$, on which different boundary conditions will be used. Here, Γ_0 represents a solid wall while Γ_∞ represents the far field (inflow or outflow).

We do not treat a boundary condition by forcing the value of a variable to a prescribed boundary value, but consider instead the integral formulation (15) and apply the boundary condition by modifying the flux integrals on $\partial\mathscr{C}_i$ for those cells such that $\Gamma \cap \partial\mathscr{C}_i \neq \varnothing$.

For example, for a vertex i located on Γ_0, we do not impose the slip condition $\mathbf{U}\cdot\mathbf{n} = 0$, but we take this condition into account in the evaluation of the convective flux,

$$\int_{\Gamma_0\cap\partial\mathscr{C}_i} Fn_x + Gn_y = \begin{bmatrix} 0 \\ \int_{\Gamma_0\cap\partial\mathscr{C}_i} pn_x \\ \int_{\Gamma_0\cap\partial\mathscr{C}_i} pn_y \\ 0 \end{bmatrix}.$$

The pressure integrals are computed as

$$\int_{\Gamma_0\cap\partial\mathscr{C}_i} pn_x \simeq p_i \int_{\Gamma_0\cap\partial\mathscr{C}_i} n_x,$$
$$\int_{\Gamma_0\cap\partial\mathscr{C}_i} pn_y \simeq p_i \int_{\Gamma_0\cap\partial\mathscr{C}_i} n_x.$$

For a vertex located on Γ_∞, we again use an approximate Riemann solver. We define a far field state W_∞, $\mathbf{n}_i = \int_{\Gamma_\infty\cap\partial\mathscr{C}_i} \mathbf{n}$ and set, in agreement with what has been done in the interior of the computational domain,

$$\int_{\Gamma_\infty\cap\partial\mathscr{C}_i} Fn_x + Gn_y = \Phi(W_i, W_\infty, \mathbf{n}_i). \tag{21}$$

In Eq. (21), Φ is a numerical flux function. For simplicity reasons, we have chosen a modified Steger–Warming flux, instead of the Roe one:

$$\Phi(W_i, W_\infty, \mathbf{n}) = A_{\mathbf{n}}^+ W_i + A_{\mathbf{n}}^- W_\infty.$$

The matrices $A_{\mathbf{n}}^+$ and $A_{\mathbf{n}}^-$ are the positive and negative parts of the matrix $A_{\mathbf{n}}$ defined in (14) and evaluated for $W = W_i$.

In all the examples we have treated below, the boundary here was either fully subsonic or fully supersonic, so that the procedure was really simple, contrary to what would have been added in mixed type boundary conditions.

Finally, we have reduced the order of accuracy of the reconstruction for cells that are too near the boundary. For

them, a proper calculation of the ENO stencil may be impossible because the set of possible stencils is biased in one direction due to the boundary. For the third-order scheme, these cells are those related to a mesh point that belongs to a triangle having at least one point on the boundary. For the fourth-order scheme, they are those belonging to a triangle, a vertex of which is related to a cell for which a reduction of order must be done for the third order.

3.3. Positivity of the Density and the Pressure

As pointed out by Harten *et al.* [23], in some situations and for extremely few cells, the ENO reconstruction of the density and pressure may lead to negative values. For these cells, and these cells only, following [23], we reduce the order of accuracy with the following inductive method (w is either the density or the pressure; w_i is its average on $\mathcal{C}_i$). Consider, in $\mathcal{C}_i$, the reconstruction

$$R(w, n)(X, Y) = \sum_{l=0}^{n} \sum_{p+q=l} a_{pq}(X-x_g)^p (Y-y_g)^q.$$

If $\sum_{l=2}^{n} \sum_{p+q=l} |a_{pq}| \, |(x-x_g)^p (y-y_g)^q| \geqslant \alpha |w_i|$ at a Gaussian point (x, y), then the reconstruction, for that point, is set to $R(w, n-1)(x, y)$. Then, we repeat the test if necessary. Usually, the parameter α is set to 0.95.

In all the simulations we have done, the tests were positive for a very small set of cells and a zeroth-order reconstruction was never used. They were never positive for the second-order scheme. This number is problem dependent. For example, only at most three points caused problems from time to time for the facing step problem with a 5000-node mesh. They all were located in the front shock.

4. NUMERICAL TESTS

All the examples we propose now have been computed with the second and third ENO schemes. The ratio of specific heats, γ, is always set to 1.4.

4.1. A Linear Advection Problem

In order to test the precision of these schemes, we have computed the advection of a sine wave on different totally unstructured meshes with an increasing number of points. The convection velocity was parallel to the x axis but since the meshes are totally unstructured, there is no privileged direction. Figure 5 shows, in the abscissa, the logarithm of the maximum radius of the circumscribed circles of the triangles of the meshes, and, in the ordinate, the logarithm of the maximum absolute value of the difference between the computed and the exact solution. The slopes -2 and -3 are indicated, so that one can see that the expected order of accuracy is indeed achieved.

4.2. A Shock Tube Problem

We have set up a two-dimensional shock tube problem in the square $[0, 1] \times [0, 1]$. Its boundary are solid. The initial conditions are:

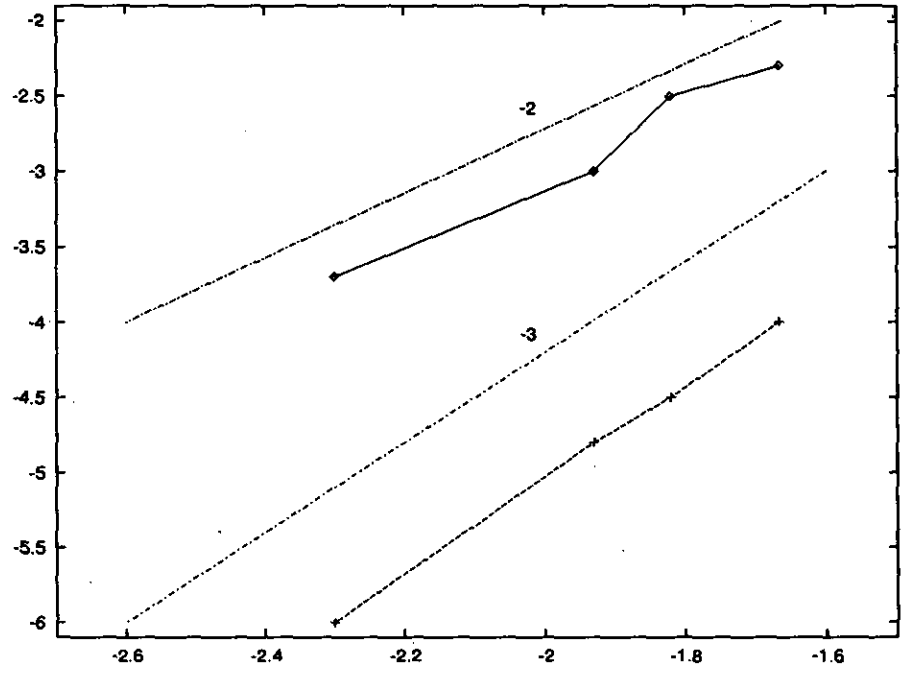

FIG. 5. Representation of the logarithm of the L_∞ error in term of the logarithm of the maximum radius of the circumcircles.

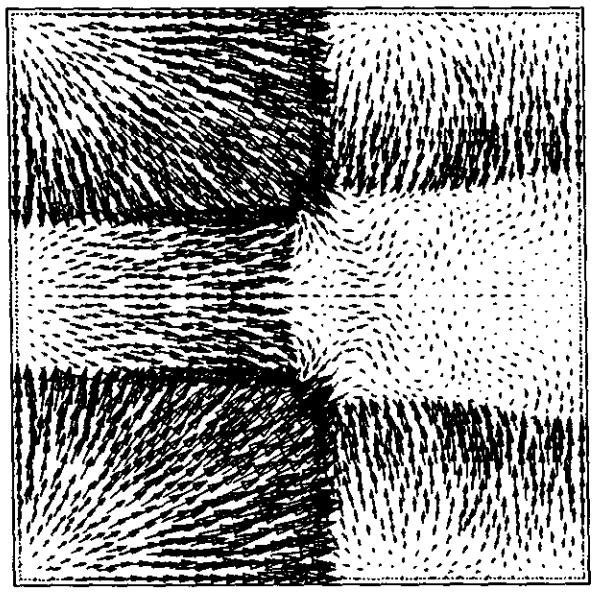

FIG. 6. Shock tube: velocity field at time $t = 0.9$.

If $x \leqslant 0.5$ and $|y - 0.5| \leqslant 0.25$,

$$\rho = 1,$$
$$u = v = 0,$$
$$p = 1,$$

else

$$\rho = 0.125,$$
$$u = v = 0.0,$$
$$p = 0.1.$$

The mesh is completely unstructured with 2127 nodes and 4088 triangles. The velocity field obtained by the third-order

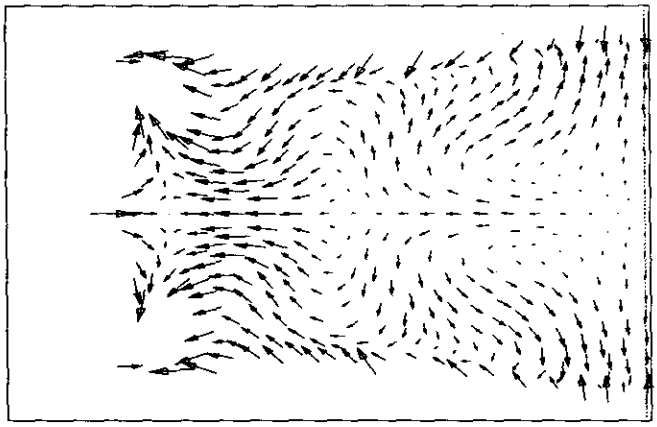

FIG. 7. Zoom of the velocity field in $[0.5, 1] \times [0.25, 0.75]$. Second-order solution.

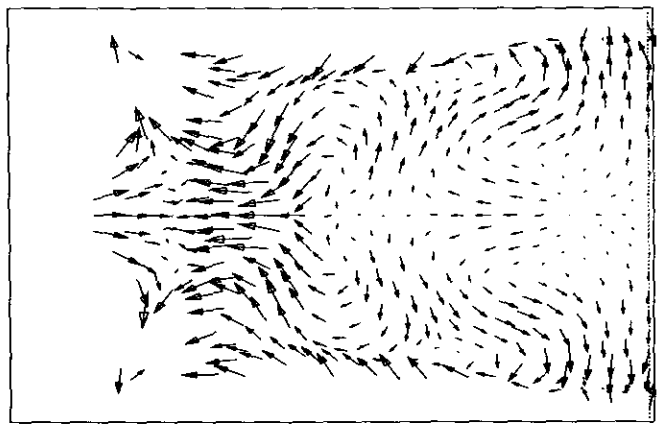

FIG. 8. Zoom of the velocity field in $[0.5, 1] \times [0.25, 0.75]$. Third-order solution.

scheme at time $t = 0.9$ is displayed in Fig. 6. The differences between both results are more clearly visible in the near stagnation zone. In order to represent that area better, we have removed from the velocity field all the points for which the sum of the absolute values of its two components is larger than 0.15. The result is shown on Figs. 7 (second order) and 8 (third order). One can clearly observe that the number of small structures of the flow are much more important in Fig. 8 than in Fig. 7. The shocks in the upper and lower parts of the pictures also have a different resolu-

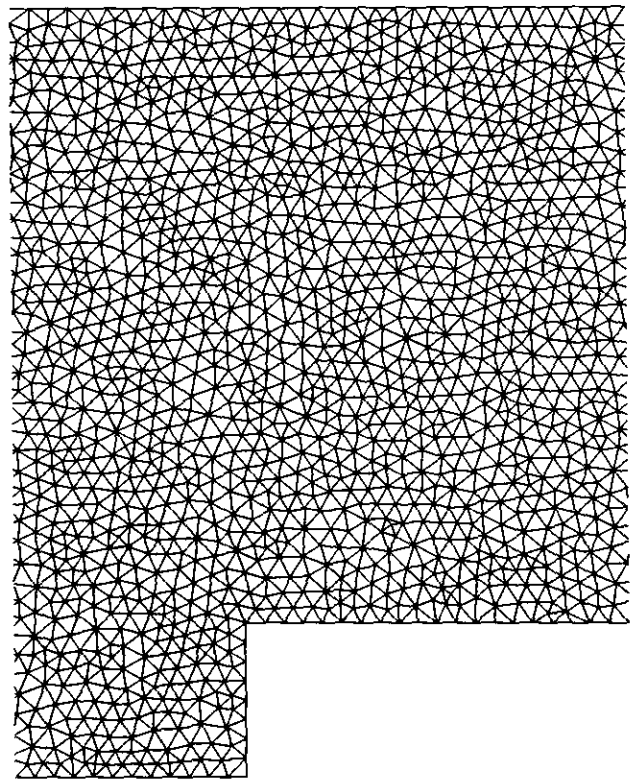

FIG. 9. Portion of the mesh used for the step case.

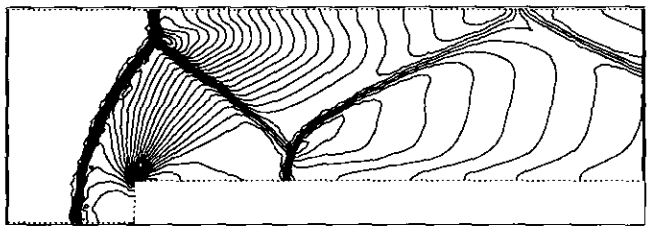

FIG. 10. Density contours for the second-order ENO solution, $t = 4$, min = 0.329, max = 4.64. Density contours from 0.287 to 4.584, $\Delta\rho = 0.14$.

tion. Their location is also different but this can be seen only by superimposing the pictures.

One should also mention that this test is not particularly easy for our method. After a few time steps, the shock reflects with the wall. The reflected shock interacts with the other structures of the flow, leading to interactions between the various kinds of discontinuities and with the smooth parts of the flow. The multiple points, as shown on our figures, with different kind of discontinuities (contact and shock) are resolved by our method without any particular trick.

4.3. A Mach 3 Wind Tunnel with a Step

We have run this test case, that is well documented in [24], for the second-order and third-order ENO schemes on a 5140 node and 9958 triangle mesh. This discretization corresponds to the medium mesh used in [24]. A portion of it is displayed in Fig. 9. It is totally unstructured. The conditions of the problem are the following: a uniform Mach 3 flow is set in a channel. At the initial time, a step of relative height 0.2 is installed in it. The channel length is 3 and the step is located at 0.6. This situation creates a shock that reflects on the upper part of the channel; then it evolves to a lambda shock as the time increases. It interacts with the upper part of the step. A weak shock is also created by the expansion wave at the corner. This shock interacts with the reflected one, creating a slip line. The location of this slip line is very dependent on the boundary conditions that are set at the corner.

Here, no special treatment is done, contrary to what is advocated in [24], so that the quality of the second

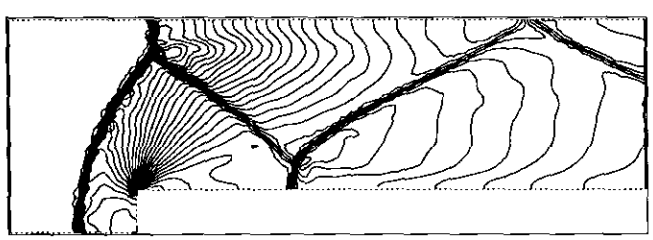

FIG. 11. Density contours for the third-order ENO solution, $t = 4$, min = 0.287, max = 4.584, $\Delta\rho = 0.14$.

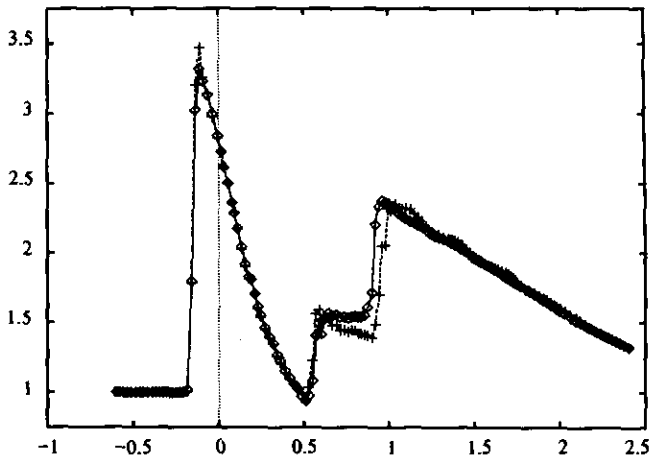

FIG. 12. Cross section of the density, $y = 0.5$: $\diamond$, second order; $+$, third order.

reflected shock is poor. We only want to verify the effect of the increasing order of accuracy on the solution, so that we will only look at the first reflected shock. The solutions of Fig. 10 (second-order ENO) and Fig. 11 (third-order ENO) are shown. A clear improvement on the thickness of that reflected shock can clearly be seen from the horizontal cross section of the density at $y = 0.5$, Fig. 12. The slip line coming from the lambda shock is also more visible in Fig. 11 than in Fig. 10, as well as the weak shock near the corner.

4.4. Reflection of a Shock on a Wedge

This problem is also well documented in the literature. In order to achieve a correct solution, one has either to use very fine meshes or adapted meshes (see [5], for example). We have chosen a case where the planar shock enters from the left in a quiescent fluid. Its Mach number is $M_S = 5.5$ and is defined towards the flow values in the quiescent fluid where the density is set to 1.4 and the pressure to 1. One expects a double Mach reflection.

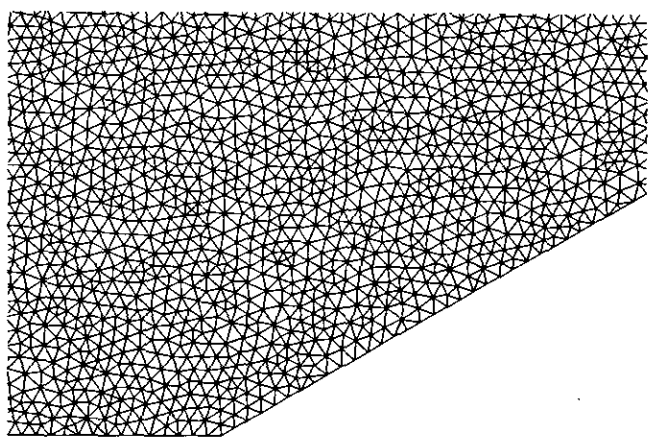

FIG. 13. Portion of the mesh used for the Mach reflection problem.

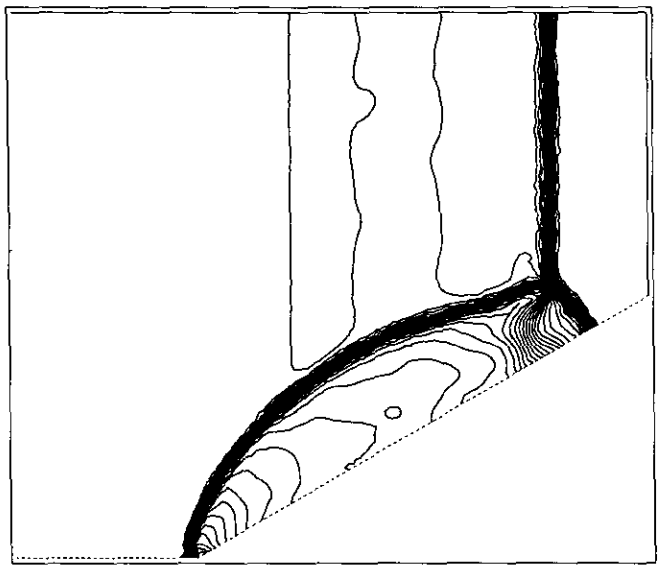

FIG. 14. Refection of a planar shock by a wedge: density contours, second-order solution. Min = 1.4, Max = 17.3. Contour from 1.4 to 19.088, $\Delta\rho = 0.36$.

The mesh has only 8569 points and 16806 triangles. A part of it is shown in Fig. 13. The density contours of the two calculations are displayed in Fig. 14 (second order) and Fig. 15 (third order). A very clear improvement of the slip line coming from the Mach stem can be observed. The second triple point can also been observed in Fig. 15, although it is of poor quality because of the insufficient resolution of the present mesh, but it is totally indistinguishable in Fig. 14. Generally speaking, all the discontinuities are better resolved by the third-order scheme.

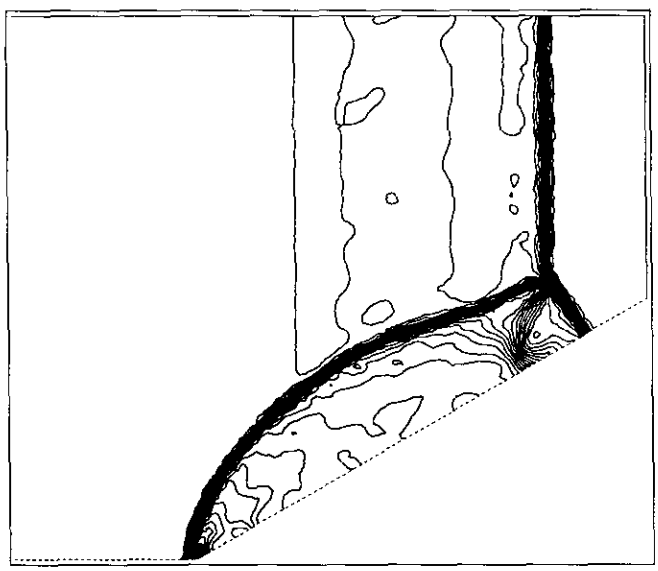

FIG. 15. Refection of a planar shock by a wedge: density contours, third-order solution. Min = 1.4, Max = 19.0088, $\Delta\rho = 0.36$.

5. CONCLUSIONS

A third-order ENO scheme has been derived on triangular type unstructured meshes; this demonstrates that deriving ENO schemes on unstructured meshes is something possible. We indicate how to build higher order ENO schemes and give some comments on the numerical stability of the reconstruction step.

This new scheme has been tested on a set of well-known test cases and compared to a second-order one. In all cases, the results are clearly improved. Our results also demonstrate its robustness. The cost of the scheme is four times that of the second-order one (on a Cray YMP) but the code is far from being optimized. In particular, no effort has been made in the ENO reconstruction procedure, the most expensive routine, so that this ratio can be considered as a bad upper bound.

In the near future, we will derive the fourth-order version of this class of schemes. The two schemes will be coupled with a dynamic adaptation procedure [3] to improve its efficiency.

ACKNOWLEDGMENTS

I am very much indept of encouraging discussions I had with A. Harten, S. W. Shu, J. J. Quirck, and J. Casper during my stay at ICASE. My colleagues A. Dervieux and H. Guillard are also acknowledged. This research was partly conducted while the author was in residence at ICASE, Hampton, Virginia under Contract No. NAS1-19480.

REFERENCES

1. H. C. Yee, Technical Report TM-89464, NASA, May 1987 (unpublished).
2. L. Fezoui and B. Stoufflet, *J. Comput. Phys.* **84**(1), 174 (1989).
3. N. Maman and B. Larrouturou, "Dynamical Mesh Adaptation for Two-Dimensional Reactive Flow Simulation," in *Numerical Grid Generation in Computational Fluid Dynamics and Related Field*, edited by A. S. Arcilla, J. Häuser, P. R. Eiseman, and J. F. Thompson, (Elsevier Science, New York, 1991), p. 13.
4. B. Palmerio and A. Dervieux, in *13th IMACS World Congress on Computation and Applied Mathematics, July 22–26, 1991, Dublin, Ireland*, to appear.
5. J. J. Quirk, ICASE Report 92-7, February 1992 (unpublished).
6. A. Harten and S. Osher, *SIAM J. Numer. Anal.* **24**(2), 279 (1987).
7. A. Harten, S. Osher, B. Engquist, and S. R. Chakravarthy, "Some Results on Uniformly High-Order Accurate Essentially Nonoscillatory Schemes," in *Applied Numerical Analysis Vol. 2* (Elsevier Science, North Holland, New York, 1986), p. 347.
8. A. Harten, B. Engquist, S. Osher, and S. R. Chakravarthy, *J. Comput. Phys.* **71**, 231 (1987).
9. C. W. Shu and S. Osher, *J. Comput. Phys.* **77**, 439 (1988).
10. A. Harten, *J. Comput. Phys.* **83**, 148 (1989).
11. J. Casper and H. L. Atkins, *J. Comput. Phys.* **106**, 62 (1993).

12. R. Abgrall, ICASE Report 91-84, December 1991; revised form, INRIA Report No. 1592, January 1992; *Math. Comput.*, submitted.
13. R. Abgrall, in *Proceedings, Second International Conference on High Order and Spectral Methods, June 22–26, 1992*; *Comput. Methods Appl. Mech. Eng.*, to appear, 1994.
14. A. Harten and S. R. Chakravarthy, ICASE Report No. 91-76, September 1991; *J. Comput. Phys.*, submitted.
15. S. R. Chakravarthy, K.-Y. Szema, and C.-L. Chen, AIAA Paper 91-3340 (unpublished).
16. P. Vankeirsblick and H. Deconinck, Paper No. 7, AGARD R-787, May 1992 (unpublished).
17. T. J. Barth and P. O. Frederickson, AIAA Paper No. 90-0013, 28th Aerospace Science Meeting, January 8–11, 1990, Reno, Nevada (unpublished).
18. K. C. Chung and T. H. Yao, *SIAM J. Numer. Anal.* **14**(4), 735 (1977).
19. G. Muhlbach, *Numer. Math.* **32**, 393 (1979).
20. G. Muhlbach, *Numer. Math.* **31**, 97 (1978).
21. G. Strang and G. J. Fix, *An Analysis of the Finite Element Method* (Prentice-Hall, Englewood Cliffs, NJ, 1973).
22. P. G. Ciarlet and P. A. Raviart, *Arch. Rat. Mech. Anal.* **42**, 177 (1972).
23. A. Harten, B. Engquist, S. Osher, and S. K. Chakravarthy, ICASE Report 86-22, April 1986 (unpublished).
24. P. Woodward and P. Colella, *J. Comput. Phys.* **54**, 115 (1984).